CHINESE OPTICS LETTERS

Vol. 21, No. 10 | October 2023

Wavelength and polarization dual-multiplexed imaging based on holographic metasurfaces

Jilian Xu (许继莲), Zhiyuan Yue (岳智远), Peiyao Lu (路佩遥), Rui Wu (武 瑞), Kun Jiang (姜 昆), Xiquan Jiang (蒋喜全), and Shuyun Teng (滕树云)*

Shandong Provincial Engineering and Technical Center of Light Manipulations & Shandong Provincial Key Laboratory of Optics and Photonic Device, School of Physics and Electronics, Shandong Normal University, Jinan 250014, China

*Corresponding author: tengshuyun@sdnu.edu.cn

Received March 13, 2023 | Accepted May 11, 2023 | Posted Online October 3, 2023

In light of the powerful light manipulation ability of holographic metasurfaces, optical imaging with wavelength multiplexing and polarization multiplexing is performed in this paper. The metasurface is composed of identical rectangular nanoholes etched in silver film. Three imaging effects, including the in-plane color imaging, three-dimensional wavelength-encrypted imaging, and polarization-multiplexing wavelength-encrypted imaging, are realized. The designed metasurface has compact structure, and the obtained image has lower noise. The simulation and experiment results give the verification. Multiple images, including spatial multiplexing, wavelength multiplexing, and polarization multiplexing, exhibit immense potentialities of metasurfaces, and this work is helpful for expanding the applications of metasurfaces.

Keywords: metasurface; holography; optical encryption; color imaging.
DOI: 10.3788/COL202321.100501

1. Introduction

Metasurface holography is a progressive technique that combines computer-generated holographic imaging and metasurface structure[1–3]. The high spatial resolution in the nanometer scale, the ultra-thin structure with sub-wavelength thickness, and the extensive information capacity of the holographic metasurface enable metasurface holography to be competent in more applied fields, especially nanophotonics and integrated optics[4,5]. Therefore, metasurface holography has attracted much attention in recent years, and it has been applied in holographic imaging[6,7], information encoding[8,9], nanometer ptychography[10], and other light field manipulations[11,12].

Holographic metasurfaces manipulate the light field by changing the shape and size of nanounits and their arrangement in space. Metasurface holograms may be obtained in terms of the geometric phase[13–15], the propagation phase[16,17], and the resonant phase[2,18] introduced by nanounits. Resonant metasurfaces have a relatively higher working efficiency and geometric metasurface, which can be achieved only through rotating nanounits, and have more flexible phase control[19]. The reflective geometric metasurfaces based on a metal-dielectric-metal design and a dielectric material are proposed to increase the efficiency of the geometric metasurface[13,20]. Meanwhile, the transmission geometric metasurfaces are still widely used because of the convenient operation and the large signal-to-noise ratio[15,21].

In addition to the simple imaging that is based on metasurface holography, controllable multiple imaging is also achieved based on a holographic metasurface. The incident angle[22,23], the state of polarization[24–26], the wavelength[27–29], and the orbital angular momentum[30,31] of the illuminating light may be used to control the holographic imaging. The angle multiplexing metasurfaces show the different responses of the phase and the amplitude to different illumination angles, and can generate independent nano-printing and meta-holography for different illumination angles[23]. The polarization-multiplexing metasurface consisting of interlaced nanounits is used to generate different images with orthogonal linearly or circularly polarized light illumination[24,26,32]. The motion pictures controlled by the orbital-angular-momentum are achieved using a combination of metasurface holography and orbital-angular-momentum holography[30].

The illuminating wavelength is also used to control metasurface holographic imaging[28,33,34]. Since a specific nanounit has different wavelength responses, more sets of nanounits are usually interlaced to realize holographic color imaging. Naturally, the supercell consisting of several interlaced nanounits limits the spatial resolution[27,29,34]. Therefore, a metasurface consisting of identical simple nanounits is attractive in the design of holographic metasurfaces. Wan *et al.* reconstructed color images containing three primary colors and their secondary colors using a meta-hologram with a single type of plasmonic pixel[28]. Li *et al.* reconstructed color images with three primary colors

© 2023 Chinese Optics Letters

and seven colors also using a meta-hologram with a single type of plasmonic pixel[33], where the tilted incident angle or off-axial illumination was introduced to overcome the crosstalk among different colors. Indeed, the wavelength working with other parameters of the light field can be used to control and encrypt the light field in addition to the primary color imaging.

In this paper, we study the wavelength and polarization multiplexing imaging using a transmission holographic metasurface consisting of identical nanoholes. The rotated nanoholes are used to construct metasurface holograms, and the traditional in-plane color imaging, three-dimensional wavelength-encrypted imaging, and polarization-multiplexing wavelength-encrypted imaging are realized. The phase information of any metasurface hologram is obtained based on the Gerchberg–Saxton (G–S) algorithm. The simulation and measurement results verify the performance of the metasurface holographic imaging. In comparison to the previous research, our design does not need incline illumination[28] and avoids twin images[35]. The single metasurface can be used not only to realize in-plane imaging[36] but also to obtain three-dimensional wavelength-encrypted imaging. The advantages of simple structure, lower noise, large information capacity, and high precision may expand the broad applications of holographic metasurfaces in the fields of optical encryption, color imaging, and information storage.

2. Design Principle

Here, Fresnel holography is used to achieve the recording and reproduction of the target pattern. The Fresnel diffraction of one target with the expression of $U_0(x_0, y_0) = a\ \exp(j\varphi_0)$ can be written as the convolution of the target function and the point spread function,

$$U(x,y) = \iint U_0(x_0,y_0)H(x-x_0,y-y_0)\mathrm{d}x_0\mathrm{d}y_0 = U_0(x,y)*H(x,y), \tag{1}$$

where $k = 2\pi/\lambda$ is the wave number with λ denoting the wavelength of the illuminating light, $H(f,g) = \exp(jkz)\exp[jk(f^2+g^2)/2z]/(j\lambda z)$ represents the point spread function for the Fresnel diffraction with the propagation distance of z, and the denotation of $*$ denotes the convolution operation. This diffraction field can be also written as $U(x,y) = b\ \exp(j\varphi)$ with b and φ denoting the amplitude and phase of the diffraction field. Similarly, the inverse Fresnel diffraction of $U(x,y)$ can be also expressed in the convolution form,

$$U_f(x_r,y_r) = \iint U(x,y)H(x_r-x,y_r-y)\mathrm{d}x\mathrm{d}y = U(x_r,y_r)*H(x_r,y_r). \tag{2}$$

Inserting Eq. (1) into Eq. (2) and performing the integration operation, one can easily obtain the following relation:

$$U_f(x_r,y_r) = U_0(x_0,y_0)/(\lambda z)^2. \tag{3}$$

Obviously, the result of Eq. (3) is the same as the target function except for the constant term. This indicates that the diffraction field is just the image of the target. Naturally, while the holographic diagram is formed based on the Fresnel diffraction of one target, the image of the target will appear as the holographic diagram is illuminated by the light with the wavelength of λ.

Here, we use phase-only holography to reproduce the image of the target, and the hologram is obtained with the help of the G–S algorithm. In this algorithm, the Fresnel transformation (FrT) of the object wave adding the random initial phase is performed, as shown in Fig. 1(a). Then, the reverse Fresnel transformation (RFrT) is implemented with only remaining the phase term of the diffraction field. While the error between the reproduced image and the target is smaller than the defaulted value, the hologram is output. Otherwise, the initial phase is replaced by the diffraction phase φ', and the FrT and RFrT are performed again until the reproduced image meets the requirement. The iteration times for the G–S algorithm depend on the calculation error.

The above analysis is for a specific wavelength. The actual color imaging corresponds to different wavelengths. The targets for three wavelengths are different, like the ones of a_1, a_2 and a_3, and their diffraction fields through three FrTs can be expressed by $b_1\ \exp(j\varphi_1)$, $b_2\ \exp(j\varphi_2)$, and $b_3\ \exp(j\varphi_3)$. The RFrTs with only remaining the phase term of $b\ \exp(j\varphi) = b_1\ \exp(j\varphi_1) + b_2\ \exp(j\varphi_2) + b_3\ \exp(j\varphi_3)$ are conducted. The phase φ is output while the errors between three reproduced images and their targets are smaller than the defaulted values. Otherwise, the loop operations for FrT and RFrT are repeated. The G–S algorithm for multiple-wavelength imaging is shown in Fig. 1(b). The

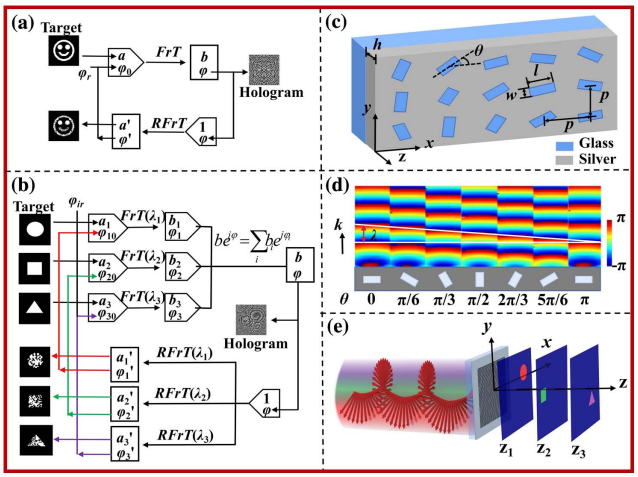

Fig. 1. (a) The G–S algorithm of the typical hologram, (b) the G–S algorithm for the multiple-wavelength hologram, (c) the schematic diagram of the metasurface, (d) the transmission phase distributions of the rotated nanoholes, and (e) the reproduction for target images based on the metasurface hologram.

reproduced images for the three wavelengths can be written in the following form,

$$U_f(x_r, y_r) = \frac{U_{01}(x_{01}, y_{01})}{(\lambda_1 z_1)^2} + \frac{U_{02}(x_{02}, y_{02})}{(\lambda_2 z_2)^2} + \frac{U_{03}(x_{03}, y_{03})}{(\lambda_3 z_3)^2}, \tag{4}$$

where z_1, z_2, and z_3 are the positions of the target images for the three wavelengths. As $z_1 = z_2 = z_3$, it is just the common in-plane color imaging. As $z_1 \neq z_2 \neq z_3$, it corresponds to the three-dimensional holographic imaging with wavelength encryption. As $\lambda_1 = \lambda_2 = \lambda_3$, $z_1 \neq z_2 \neq z_3$, or $x_{01} \neq x_{02} \neq x_{03}$, or $y_{01} \neq y_{02} \neq y_{03}$, it is the spatial multiplexing holographic imaging.

The metasurface hologram can realize the phase control using the spatially varying nanounits, and the nanounits in this paper are chosen as periodic rectangular nanoholes etched in silver film. Figure 1(c) shows the metasurface structure and the parameters of the metasurface, including the rotation angle, the length and width of the nanohole, the separation of two adjacent nanoholes, and the thickness of the silver film. The rotated nanohole can introduce the geometric phase shift, and it can be reflected using the transmission field in the circular polarization base[37],

$$T = A\begin{pmatrix} i_1 \\ i_2 \end{pmatrix} + Bi_2 e^{-j2\theta}\begin{pmatrix} 1 \\ 0 \end{pmatrix} + Bi_1 e^{j2\theta}\begin{pmatrix} 0 \\ 1 \end{pmatrix}, \tag{5}$$

where $A = [a_x + a_y \exp(j\delta)]/2$ and $B = [a_x - a_y \exp(j\delta)]/2$ with a_x and a_y denoting the amplitudes of transmission field along two major axes of the nanohole and δ denoting the phase difference along the two directions. The angle of θ is the rotation angle of the nanohole. The first term at the right side of Eq. (5) has the same polarization as the incident light of (i_1, i_2). The Jones vector (1, 0) denotes the left-handed circularly polarized (LCP) state, and the Jones vector (0, 1) denotes the right-handed circularly polarized (RCP) state. Obviously, the additional phase terms of $\exp(\pm j2\theta)$ are carried by two circularly polarized components. The introduced phase shift equals twice of the rotation angle of the nanohole, and the transmission phase distributions of the rotated nanohole shown in Fig. 1(d) verify this.

In order to increase the transmittance of the metasurface, to prevent the information crosstalk of the color patterns, and to meet the Nyquist sampling theorem, the structure parameters of metasurfaces need to be optimized[14]. Through the optimization, the separation of two adjacent nanoholes takes 250 nm, the length of nanohole takes 130 nm, the width takes 70 nm, and the thickness of silver film takes 150 nm. The polarization conversion efficiencies of the periodic nanoholes for three wavelengths of 633 nm, 532 nm, and 425 nm reach 55.5%, 62.9%, and 72.8%, respectively.

The Fresnel hologram for the target image can be achieved by arranging the periodic nanoholes with their rotation angles equaling half of the phases at corresponding coordinates. Figure 1(e) shows the reproduction process of the target images for different wavelengths at different propagation distances, where the illuminating light takes the LCP state. The wavelength multiplexing and spatial multiplexing holography can be implemented as the target images, and their positions change with the wavelengths. Meanwhile, color imaging can be realized as the propagation distances for target images for different wavelengths are the same.

3. Numerical Simulations

We first design the metasurface hologram to realize the reproduction of one color doll. The head, the torso, and the leg of the color doll correspond to the wavelength of 633 nm, 532 nm, and 425 nm, respectively. The color doll stitched by three parts is set at 10 μm away from the metasurface. Figure 2(a) shows a part of the designed metasurface, and its phase distribution comes from the data obtained using the G–S algorithm. Figure 2(b) shows the target pattern, and Figs. 2(c)–2(f) give the reproduced patterns when three lights simultaneously and separately illuminate the metasurface. For convenient observation, the shapes for three parts of the doll are inserted in Figs. 2(c)–2(f), and the coordinates for the three parts are labeled in Figs. 2(b) and 2(c).

From the results shown in Figs. 2(b) and 2(c), it is easy to see that the reproduced image is almost the same as the target pattern. The shapes and the positions for three parts of the reproduced doll in Figs. 2(d)–2(f) show that the target patterns can be accurately reproduced, although some lower noises still exist. These results confirm the feasibility of the theoretical analysis and the metasurface design, and one single metasurface consisting of identical nanoholes can realize the color imaging with lower noise. Similarly, changing the positions of the target patterns for different wavelengths, one can also obtain the three-dimensional wavelength-encrypted imaging.

The three targets for the three wavelengths are still set as a circle, a square, and a triangle, and their images appear at the different positions. We construct the metasurface hologram based on the data obtained using the G–S algorithm. The circle

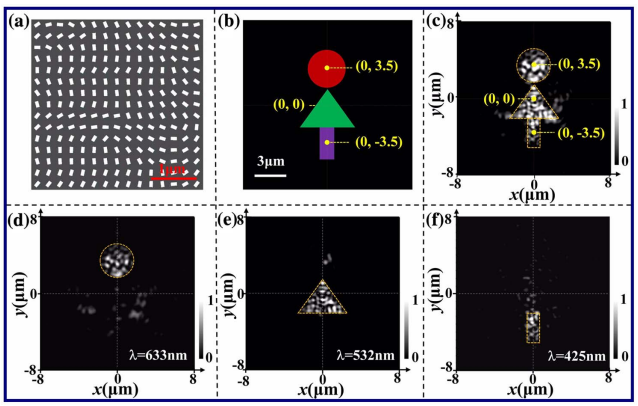

Fig. 2. (a) Part structure of the metasurface, (b) the target color doll, and the reproduced images as the metasurface is illuminated by the lights with wavelengths of 633 nm, 532 nm, and 425 nm, (c) simultaneously and (d)–(f) separately.

for the wavelength of 633 nm is set at the farthest distance, and the triangle for the wavelength of 425 nm is set at the nearest distance. This is equivalent to controllable imaging with negative dispersion. On the contrary, while the circle for the wavelength of 633 nm appears at the nearest distance, the triangle for the wavelength of 425 nm appears at the farthest distance. This is equivalent to controllable imaging with the positive dispersion[38]. Figure 3(a) shows the reproduced results for the former case with three target patterns appearing at (5.5 μm, −5.5 μm, 18 μm), (−5.5 μm, 0, 19 μm), and (5.5 μm, 5.5 μm, 20 μm), and Fig. 3(b) shows the reproduced results for the latter case with three target patterns appearing at (5.5 μm, 5.5 μm, 18 μm), (−5.5 μm, 0, 19 μm), and (5.5 μm, −5.5 μm, 20 μm).

From the results shown in Figs. 3(a) and 3(b), one can see that all the target patterns are reproduced at the positions as theoretical predictions, and the noise for the former case seems to be slightly less than that for the latter case. These results prove the effectiveness of metasurface holography in three-dimensional wavelength-encrypted imaging, and they also confirm that metasurface holography realizes wavelength multiplexing and demultiplexing.

It needs to be pointed out that all the simulations are obtained using the finite-difference time-domain technique[39]. The rectangular holes are etched in the silver film deposited on the glass substrate, and the dielectric constants of the silver for different wavelengths are given by Palik[40]. The perfectly matched layer is used as the absorption boundary to prevent the reflection of the light field from the boundary. The minimum mesh takes 2 nm so as to ensure the calculation accuracy. The dimensions of the metasurface are limited within the region of 30 μm × 30 μm. The simulation results effectively verify the in-plane color imaging and the three-dimensional wavelength-multiplexing imaging of holographic metasurfaces.

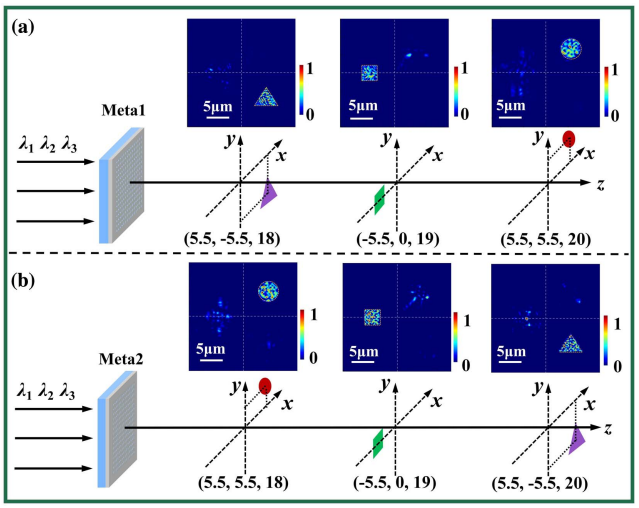

Fig. 3. Three-dimensional wavelength-multiplexing imaging with the reproduced images appearing at (a) (5.5, −5.5, 18), (−5.5, 0, 19), and (5.5, 5.5, 20) (in scale μm) for the wavelengths of 425 nm, 532 nm, and 633 nm and at (b) (5.5, 5.5, 18), (−5.5, 0, 19), and (5.5, −5.5, 20) (in scale μm) for the wavelengths of 633 nm, 532 nm, and 425 nm.

4. Experimental Measurement

In order to further verify the optical performance of the holographic metasurface, we manufacture one metasurface sample to realize three-dimensional wavelength-multiplexing imaging. We first deposit a 150-nm silver film on the glass substrate with the help of magnetron sputtering. The sputtering condition contains a sputtering rate of 0.22 nm per second, the DC sputtering power of 10 W, the vacuum degree of 1×10^{-3} Pa, and a deposition pressure of 0.5 Pa. Then, we fabricate the periodic rectangular nanoholes in the silver film using the focused ion beam etching technique, where the working voltage is set at 30 kV, and the current is set at 92 pA. Figure 4(b) shows the SEM images of the metasurface sample, which can reproduce the triangle for the wavelength of 450 nm at $z_1 = 18$ μm, the square for the wavelength of 532 nm at $z_2 = 19$ μm, and the circle for the wavelength of 633 nm at $z_3 = 20$ μm.

The metasurface sample is placed in the optical path shown in Fig. 4(a) to reproduce the target image. The light emitted from any laser passes through the polarizer (P) and the quarter-wave plate (QWP) to form LCP light. Three lights coaxially propagate with the aid of the reflector and beam splitters. Finally, three lights impinge onto the metasurface sample from the glass substrate. A charge-coupled device (CCD) receives the intensity distribution magnified by the microscope objective (MO). The other combination of the QWP and the P is used to extract the cross circular polarization component of the transmission field. For convenient measurement, the sample is placed on the translation platform with the precision of 10 nm, and three shutters (S) are placed on three light paths.

Figures 4(c)–4(e) give the measured results when the sample translates away from the metasurface, which is separately illuminated by the laser light with different wavelengths. The result in Fig. 4(c) corresponds to the nearest distance z_1, and the result in Fig. 4(e) corresponds to the farthest distance z_3. One can see that

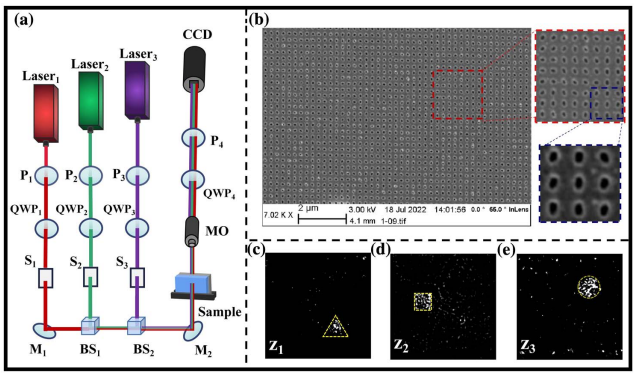

Fig. 4. (a) Experimental setup for measuring the reproduced pattern. (b) The SEM images of the metasurface sample. (c)–(e) The intensity distributions measured at different longitudinal positions with the wavelengths taking 450 nm, 532 nm, and 633 nm, respectively.

the crosstalk is almost undistinguishable. This indicates that the designed metasurface has better wavelength encryption. These experimental results are consistent with the simulation results given in Fig. 3(a). While three laser lights simultaneously illuminate the sample, the measured results are consistent with the above results. The nonuniform shapes for the experimental results come from the imperfect fabrication of the rectangular nanoholes.

5. Wavelength-Encrypted Polarization Multiplexing Imaging

For further increasing the multiplexing function of the holographic metasurface, we combine two sets of nanoholes to form one compound metasurface, and the two sets of nanoholes respond, respectively, to LCP and RCP lights. Thus, more target patterns can be reproduced using the single metasurface, where the reproduction of the target patterns is simultaneously controlled by the illuminating wavelength and the incident polarization. Figure 5(a) shows the compound metasurface interlaced by two sets of nanoholes (Interlaced-Holo), where the red nanoholes respond to the LCP light, and the yellow nanoholes respond to the RCP light.

The target patterns with respect to the wavelengths of 633 nm, 532 nm, and 425 nm are still set as a circle, a square, and a triangle. The target patterns reproduced by the red nanoholes are set at $z = 18\,\mu$m for the wavelength of 425 nm, $z = 19\,\mu$m for the wavelength of 532 nm, and $z = 20\,\mu$m for the wavelength of 633 nm. The target patterns reproduced by the yellow nanoholes are set at $z = 18\,\mu$m for the wavelength of 633 nm, $z = 19\,\mu$m for the wavelength of 532 nm, and $z = 20\,\mu$m for the wavelength of 425 nm. Figures 5(b) and 5(c) give the simulated results for the diffraction intensity distributions of this compound metasurface with the LCP and RCP light illumination. The three patterns in Fig. 5(b) from left to right are just the triangle, the square, and the circle. Three patterns in Fig. 5(c) from left to right are just the circle, the square, and the triangle. These results are consistent with the defaulted patterns.

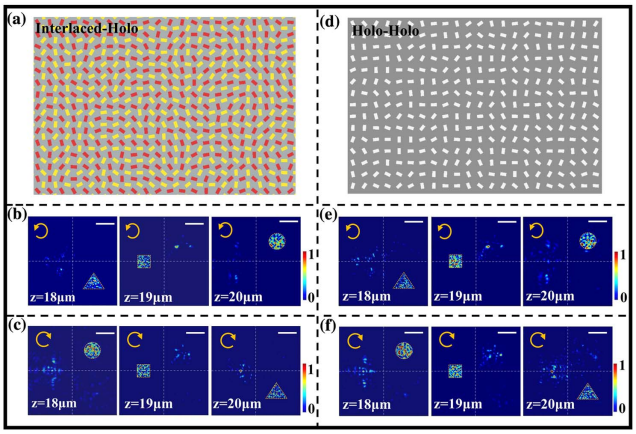

Fig. 5. Compound metasurfaces (a) interlaced by two sets of nanoholes and (d) produced by holography. Reproduced target patterns (b), (e) at $z = 18\,\mu$m for $\lambda_1 = 425$ nm, $z = 19\,\mu$m for $\lambda_2 = 532$ nm, and $z = 20\,\mu$m for $\lambda_3 = 633$ nm with LCP light illumination and (c), (f) at $z = 18\,\mu$m for $\lambda_1 = 633$ nm, $z = 19\,\mu$m for $\lambda_2 = 532$ nm, and $z = 20\,\mu$m for $\lambda_3 = 425$ nm with RCP light illumination. The inserted arrows denote the incident states of polarization, and the scale bars represent 5 μm.

Furthermore, we can construct the compound holographic metasurface using one set of nanoholes to realize the polarization multiplexing imaging. The phase information of this compound metasurface (Holo-Holo) can be obtained in terms of $\varphi_C = \arg[\exp(j\varphi_L) + \exp(-j\varphi_R)]$, where φ_L and φ_R represent the phase distributions of the two holograms for the LCP and RCP light illumination, and arg[·] means the operation for extracting the angle. Figure 5(d) shows this compound metasurface obtained in terms of the holography.

Figures 5(e) and 5(f) give the reproduced results of this compound holographic metasurface. From Fig. 5(e), one can see that the triangular pattern for the wavelength of 425 nm appears at $z = 18\,\mu$m, the square pattern for the wavelength of 532 nm appears at $z = 19\,\mu$m, and the circular pattern for the wavelength of 633 nm appears at $z = 20\,\mu$m. From Fig. 5(f), one can see that the circular pattern for the wavelength of 633 nm appears at the nearest distance, and the triangular pattern for the wavelength of 425 nm appears at the farthest distance. The reproduced images of the two metasurfaces are almost the same, and they can realize the wavelength-encrypted polarization multiplexing imaging.

6. Conclusions

In summary, we perform the wavelength-multiplexing and polarization-multiplexing imaging using a single holographic metasurface. The metasurface is composed of identical rectangular nanoholes. The in-plane color imaging, the three-dimensional wavelength-encrypted imaging, and the wavelength-encrypted polarization multiplexing imaging are achieved using the designed holographic metasurfaces. The simulation and experiment results verify the achievement of controllable holographic imaging. Compared to the previous research about color imaging, using identical nanoholes simplifies the design of the holographic metasurface, and the combination of wavelength multiplexing, spatial multiplexing, and polarization multiplexing exerts the powerful light manipulation ability of the holographic metasurface. This work shows more possibilities for the potential development of a multi-functional metasurface. The working efficiency of the metasurface may be further advanced by choosing the reflection mode and using the dielectric material. The concise design of the holographic metasurface and its parallel output are beneficial to the applications of holographic metasurfaces.

Acknowledgement

This work was supported by the National Natural Science Foundation of China (No. 10874105) and Natural Science Foundation of Shandong Province (No. ZR2020KA009).

References

1. P. Genevet and F. Capasso, "Holographic optical metasurfaces: a review of current progress," Rep. Prog. Phys. **78**, 024401 (2015).
2. Z.-L. Deng and G. Li, "Metasurface optical holography," Mater. Today Phys. **3**, 16 (2017).
3. L. Huang, S. Zhang, and T. Zentgraf, "Metasurface holography: from fundamentals to applications," Nanophotonics **7**, 1169 (2018).
4. Y. Hu, X. Luo, Y. Chen, Q. Liu, X. Li, Y. Wang, N. Liu, and H. G. Duan, "3D-Integrated metasurfaces for full-colour holography," Light Sci. Appl. **8**, 86 (2019).
5. Q. Jiang, G. Jin, and L. Cao, "When metasurface meets hologram: principle and advances," Adv. Opt. Photonics. **11**, 518 (2019).
6. L. Huang, X. Chen, H. Mühlenbernd, H. Zhang, S. Chen, B. Bai, Q. Tan, G. Jin, K.-W. Cheah, C.-W. Qiu, J. Li, T. Zentgraf, and S. Zhang, "Three-dimensional optical holography using a plasmonic metasurface," Nat. Commun. **4**, 2808 (2013).
7. L. Wang, S. Kruk, H. Z. Tang, T. Li, I. Kravchenko, D. N. Neshev, and Y. S. Kivshar, "Grayscale transparent metasurface holograms," Optica **3**, 1504 (2016).
8. L. Li, T. J. Cui, W. Ji, S. Liu, J. Ding, X. Wan, Y. B. Li, M. Jiang, C.-W. Qiu, and S. Zhang, "Electromagnetic reprogrammable coding-metasurface holograms," Nat. Commun. **8**, 197 (2017).
9. F. Dong and W. Chu, "Multichannel-independent information encoding with optical metasurfaces," Adv. Mater. **31**, 1804921 (2019).
10. Q. Song, A. Baroni, R. Sawant, P. Ni, V. Brandli, S. Chenot, S. Vézian, B. Damilano, P. de Mierry, S. Khadir, P. Ferrand, and P. Genevet, "Ptychography retrieval of fully polarized holograms from geometric-phase metasurfaces," Nat. Commun. **11**, 2651 (2020).
11. W. Ye, F. Zeuner, X. Li, B. Reineke, S. He, C.-W. Qiu, J. Liu, Y. Wang, S. Zhang, and T. Zentgraf, "Spin and wavelength multiplexed nonlinear metasurface holography," Nat. Commun. **7**, 11930 (2016).
12. J. Sung, G.-Y. Lee, and B. Lee, "Progresses in the practical metasurface for holography and lens," Nanophotonics **8**, 1701 (2019).
13. G. X. Zheng, H. Mühlenbernd, M. Kenney, G. X. Li, T. Zentgraf, and S. Zhang, "Metasurface holograms reaching 80% efficiency," Nat. Nanotechnol. **10**, 308 (2015).
14. Z. Mou, X. Q. Lu, H. R. Lv, Y. S. Han, Q. Y. Yue, S. Y. Wang, and S. Y. Teng, "Metasurface array illuminator based on Fresnel holography," Opt. Lasers Eng. **131**, 106146 (2020).
15. Z. Mou, C. Zhou, P. Lu, Q. Yue, S. Wang, and S. Teng, "Structured vortices generated by metasurface holography," Photon Res. **9**, 2125 (2021).
16. K. H. Dou, X. Xie, M. B. Pu, X. Li, X. L. Ma, C. T. Wang, and X. G. Luo, "Off-axis multi-wavelength dispersion controlling metalens for multi-color imaging," Opto Electron. Adv. **3**, 190005 (2020).
17. B. Xiong, Y. Xu, J. Wang, L. Li, L. Deng, F. Cheng, R.-W. Peng, M. Wang, and Y. Liu, "Realizing colorful holographic mimicry by metasurfaces," Adv. Mater. **33**, 2005864 (2021).
18. F. Zhou, Y. Liu, and W. Cai, "Plasmonic holographic imaging with V-shaped nanoantenna array," Opt. Express **21**, 4348 (2013).
19. P. Lu, C. Zhou, Z. Mou, D. Liu, and S. Teng, "Performance analysis of metalenses based on three kinds of phase compensation techniques," Nanomaterials **11**, 2091 (2021).
20. Z. Ma, Y. Li, Y. Li, Y. Gong, S. A. Maier, and M. Hong, "All-dielectric planar chiral metasurface withgradient geometric phase," Opt. Express **26**, 6067 (2018).
21. X. Ni, A. V. Kildishev, and V. M. Shalaev, "Metasurface holograms for visible light," Nat. Commun. **4**, 2807 (2013).
22. S. M. Kamali, E. Arbabi, A. Arbabi, Y. Horie, M. S. Faraji-Dana, and A. Faraon, "Angle-multiplexed metasurfaces: encoding independent wavefronts in a single metasurface under different illumination angles," Phys. Rev. X **7**, 041056 (2017).
23. S. Wan, C. Wan, C. Dai, Z. Li, J. Tang, G. Zheng, and Z. Li, "Angular-multiplexing metasurface: building up independent-encoded amplitude/phase dictionary for angular illumination," Adv. Opt. Mater. **9**, 2101547 (2021).
24. W. T. Chen, K.-Y. Yang, C.-M. Wang, Y.-W. Huang, G. Sun, I.-D. Chiang, C. Y. Liao, W.-L. Hsu, H. T. Lin, S. Sun, L. Zhou, A. Q. Liu, and D. P. Tsai, "High-efficiency broadband meta-hologram with polarization controlled dual images," Nano Lett. **14**, 225 (2014).
25. R. Zhao, B. Sain, Q. Wei, C. Tang, X. Li, T. Weiss, L. Huang, Y. Wang, and T. Zentgraf, "Multichannel vectorial holographic display and encryption," Light Sci. Appl. **7**, 95 (2018).
26. W. P. Wan, W. H. Yang, H. Feng, Y. L. Liu, Q. H. Gong, S. M. Xiao, and Y. Li, "Multiplexing vectorial holographic images with arbitrary metaholograms," Adv. Opt. Mater. **9**, 2100626 (2021).
27. Y.-W. Huang, W. T. Chen, W.-Y. Tsai, P. C. Wu, C.-M. Wang, G. Sun, and D. P. Tsai, "Aluminum plasmonic multi-color meta-hologram," Nano Lett. **15**, 3122 (2015).
28. W. W. Wan, J. Gao, and X. Yang, "Full-color plasmonic metasurface holograms," ACS Nano **10**, 10671 (2016).
29. B. Wang, F. Dong, Q.-T. Li, D. Yang, C. Sun, J. Chen, Z. Song, L. Xu, W. Chu, Y.-F. Xiao, Q. Gong, and Y. Li, "Visible-frequency dielectric metasurfaces for multiwavelength achromatic and highly dispersive holograms," Nano Lett. **16**, 5235 (2016).
30. H. Ren, X. Fang, J. Jang, J. Bürger, J. Rho, and S. A. Maier, "Complex-amplitude metasurface-based orbital angular momentum holography in momentum space," Nat. Nanotechnol. **15**, 948 (2020).
31. H. Zhou, B. Sain, Y. Wang, C. Schlickriede, R. Zhao, X. Zhang, Q. Wei, X. Li, L. Huang, and T. Zentgraf, "Polarization-encrypted orbital angular momentum multiplexed metasurface holography," ACS Nano **14**, 5553 (2020).
32. D. Wen, F. Yue, G. Li, G. Zheng, K. Chan, S. Chen, M. Chen, K. F. Li, P. W. H. Wong, K. W. Cheah, E. Y. B. Pun, S. Zhang, and X. Chen, "Helicity multiplexed broadband metasurface holograms," Nat. Commun. **6**, 8241 (2015).
33. X. Li, L. Chen, Y. Li, X. Zhang, M. Pu, Z. Zhao, X. Ma, Y. Wang, M. Hong, and X. Luo, "Multicolor 3D meta-holography by broadband plasmonic modulation," Sci. Adv. **2**, e1601102 (2016).
34. S. Choudhury, U. Guler, A. Shaltout, V. M. Shalaev, A. V. Kildishev, and A. Boltasseva, "Pancharatnam–Berry phase manipulating metasurface for visible color hologram based on low loss silver thin film," Adv. Opt. Mater. **5**, 1700196 (2017).
35. X. Shan, Z. Li, Q. Dai, J. Li, R. Fu, Z. He, J. Tao, and G. Zheng, "Metasurfaces with single-sized antennas for reconstructing full-color holographic images without cross talk," Opt. Lett. **46**, 5417 (2021).
36. L. Jin, Z. Dong, S. Mei, Y. F. Yu, Z. Wei, Z. Pan, S. D. Rezaei, X. Li, A. I. Kuznetsov, Y. S. Kivshar, J. K. W. Yang, and C.-W. Qiu, "Noninterleaved metasurface for (2^6–1) spin- and wavelength-encoded holograms," Nano Lett. **18**, 8016 (2018).
37. H. Wang, L. Liu, X. Lu, H. Lv, Y. Han, S. Wang, and S. Teng, "Spatial multiplexing plasmonic metalenses based on nanometer cross holes," New J. Phys. **20**, 123009 (2018).
38. Y. Han, X. Lu, H. Lv, Z. Mou, C. Zhou, S. Wang, and S. Teng, "Multi-wavelength focusing based on nanoholes," New J. Phys. **22**, 073021 (2020).
39. S. Teng, Q. Zhang, H. Wang, L. Liu, and H. Lv, "Conversion between polarization states based on a metasurface," Photonics Res. **7**, 246 (2019).
40. E. D. Palik, *Handbook of Optical Constants of Solids* (Academic, 1985).